Nanoscale

PAPER

View Article Online
View Journal | View Issue

Cite this: *Nanoscale*, 2014, **6**, 8171

Improved light absorption and charge transport for perovskite solar cells with rough interfaces by sequential deposition†

Lingling Zheng,[a] Yingzhuang Ma,[a] Saisai Chu,[a] Shufeng Wang,[ab] Bo Qu,[ab] Lixin Xiao,*[ab] Zhijian Chen,*[ab] Qihuang Gong,[a] Zhaoxin Wu[c] and Xun Hou[c]

Received 1st March 2014
Accepted 2nd May 2014

DOI: 10.1039/c4nr01141d

www.rsc.org/nanoscale

Recently, highly efficient solar cells based on organic–inorganic perovskites have been intensively reported for developing fabricating methods and device structures. Additional power conversion efficiency should be gained without increasing the thickness and the complexity of the devices to accord with practical applications. In this paper, a rough interface between perovskite and HTM was fabricated in perovskite solar cells to enhance the light scattering effect and improve the charge transport. The parameters related to the morphology have been systematically investigated by sequential deposition. Simultaneous enhancements of short-circuit current and power conversion efficiency were observed in both $CH_3NH_3PbI_3$ and $CH_3NH_3PbI_{3-x}Cl_x$ devices containing the rough interface, with power conversion efficiencies of 10.2% and 10.8%, respectively. Our finding provides an efficient and universal way to control the morphology and further optimize perovskite solar cells for devices by sequential deposition with various structures.

Introduction

Hybrid organic–inorganic perovskites, in the form of AMX_3 ($A = CH_3NH_3^+$; $M = Pb^{2+}$, or Sn^{2+}; and $X = Cl^-$, Br^-, or I^-), have attracted significant research interest in the field of solar cells. With intense absorptivity from the visible to near-infrared region, $CH_3NH_3PbI_3$ and $CH_3NH_3PbBr_3$ were firstly adopted in liquid dye-sensitized solar cells (DSSCs) as the dye-absorbing layer initiated by Miyasaka *et al.*[1] By using the organic hole transport material (HTM) of 2,2′,7,7′-tetrakis(*N*,*N*-di-*p*-methoxyphenylamine)-9,9′-spirobifluorene (spiro-MeOTAD) to avoid the dissolution of perovskite, much higher power conversion efficiencies (PCEs) have been achieved in solid-state dye-sensitized solar cells.[2,3] Recently, studies on optimizing materials, methods and device structures promoted rapid development of PCEs of perovskite solar cells.[4–23] With a new method of sequential deposition, PCE of 15% was achieved,[4] and reached 15.7% by using a thin film of ZnO nanoparticles to replace TiO_2 as the electron-transport layer.[5] The PCEs of solar cells based on perovskite are expected to push toward 20% and then beyond that of crystalline silicon (25%) through better control over all of the processing parameters.[6]

Even though the perovskite based solar cells showed effective light absorption already, additional short-circuit current (J_{sc}) and efficiency can be gained by enhancing the light absorption, especially in the long-wavelength region. H. J. Snaith *et al.* employed metal nanoparticles to reduced exciton binding energy, so that the J_{sc} improved without enhancement of light absorption.[7] M. Gräztel *et al.* used Y^{3+}-subsituted mesoporous TiO_2 to affect the crystal growth and improve the perovskite absorber loading, resulting in the higher J_{sc} and IPCE.[8] However, these methods can only be appropriate for the devices with mesoporous structure, and the use of yttrium is disadvantageous for practical applications.

It is well known that a highly roughened interface would strengthen internal light scattering, and the larger crystallites and interface area also benefit the charge transport.[5,24–26] In this paper, we adjusted the planar perovskite/HTM interface into a rough interface intending to improve the light harvesting and charge transport (Fig. 1). It was found that the reaction temperature and pre-wetting time had a great impact on the morphology of the perovskite film by sequential deposition. Under the conditions of higher reaction temperature and shorter pre-wetting time, a roughly continuous surface of densely arranged perovskite crystallites with larger size was

[a]*State Key Laboratory for Mesoscopic Physics and Department of Physics, Peking University, Beijing 100871, China. E-mail: lxxiao@pku.edu.cn; zjchen@pku.edu.cn*

[b]*New Display Device and System Integration Collaborative Innovation Center of the West Coast of the Taiwan Strait, Fuzhou 350002, China*

[c]*Key Laboratory of Photonics Technology for Information, Key Laboratory for Physical Electronics and Devices of the Ministry of Education, Department of Electronic Science and Technology, School of Electronic and Information Engineering, Xi'an Jiaotong University, Xi'an, 710049, China*

† Electronic supplementary information (ESI) available: SEM images of $CH_3NH_3I_{3-x}Cl_x$ at different reaction temperatures; SEM images of perovskite on compact TiO_2 at different reaction temperatures; AFM 3D topographic images and calculated roughness; stability of devices; and performance of each device. See DOI: 10.1039/c4nr01141d

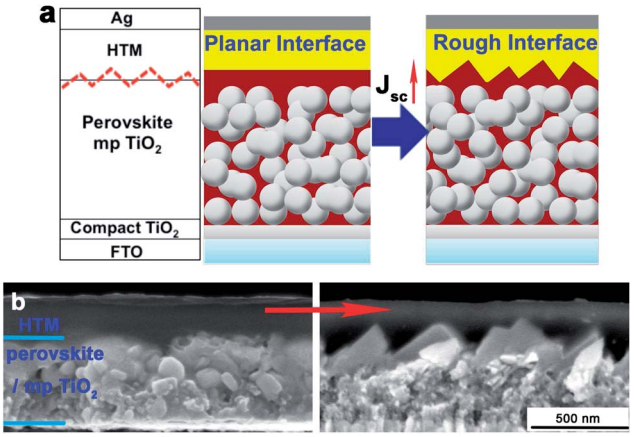

Fig. 1 (a) Structure diagram of the perovskite solar cell with a perovskite/HTM interface differed from planar to rough. (b) The cross-sectional SEM images of devices with a perovskite/HTM interface differed from planar to rough.

formed. Simultaneous increases of J_{sc} and PCE were achieved for both $CH_3NH_3PbI_3$ and $CH_3NH_3PbI_{3-x}Cl_x$ ($x \approx 0.5$) based solar cells, with the PCEs of 10.2% and 10.8%, respectively.

Results and discussion

In the sequential deposition method, the reaction between PbI_2 and CH_3NH_3I and the crystallization of perovskite happen simultaneously. So, different from the light scattering caused by nanostructures on the grid electrode,[27,28] the morphology of perovskite films can be controlled conveniently by changing the reaction and crystallization conditions. Considering the kinetics of crystal growth, both the crystallization temperature and the pre-wetting step have a great impact on the crystal size and surface roughness of the resultant film.[29] Therefore, both these ways were adjusted accurately to make the expected rough interface.

1. Reaction temperature control

The crystal size can be controlled by the reaction temperature. It was found that at a higher temperature, the crystals were inclined to grow into larger size from the solution due to the faster rate of grain boundaries' migration.[29] In order to fabricate perovskite films with different surface roughnesses, we drenched the prepared PbI_2–TiO_2 films into CH_3NH_3I solution kept at 25 °C (Film A) and 50 °C (Film B), respectively. The scanning electron microscopy (SEM) images from different views of Films A and B are shown in Fig. 2.

The SEM images showed that the perovskite crystallites not only filled the mesoporous TiO_2 but also covered it as a continuous layer. With the increase of the reaction temperature, perovskite crystallites with an in-plane grain size of 200 nm in Film A (Fig. 2a) enlarged to 350 nm in Film B formed at 50 °C (Fig. 2b), leading to a much rougher surface. Tapping-mode atomic force microscopy (AFM) was also employed to obtain more details of the surface morphology. From the 3D

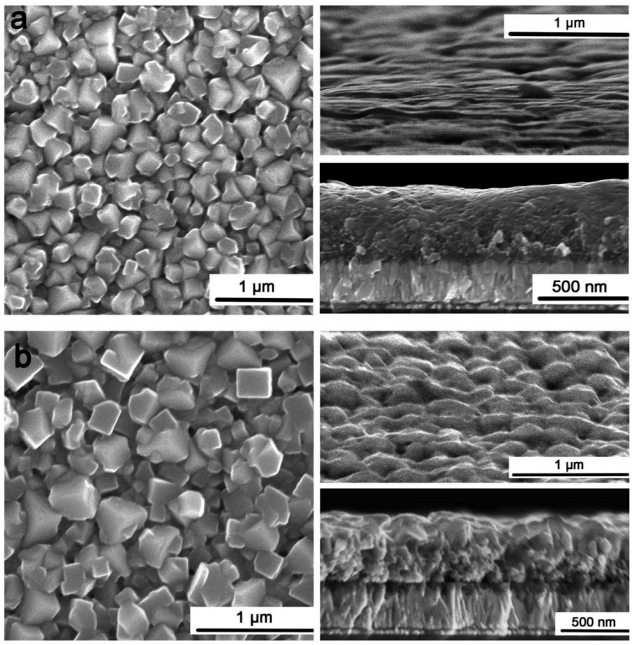

Fig. 2 Top-view, side-view, and cross-sectional SEM images of the perovskite layer on top of the mesoporous TiO_2 for (a) Film A and (b) Film B.

topographic images (Fig. S3a†), a much rougher surface of Film B was clearly observed and the calculated root mean square (rms) roughness of Film B reached 78.2 nm, much greater than 44.5 nm of Film A by analyzing the height images (Fig. S3c†).

The absorption spectra showed that Film B has stronger light harvesting from 490 nm to 800 nm than Film A (Fig. 3a), while in 350–490 nm, they have comparable absorptive intensity. This indicates the same perovskite quantity in the two films, thus the additional absorption results from the efficient light scattering effect of the rough surface. The effective optical path length of device has increased by the textured surface of large perovskite crystallites.[5] Moreover, the charge transporting property can also be improved in Film B. Firstly, the continuous crystallites with larger size enhanced the degree of ordering inside the film,[30] so that the excellent transporting properties of perovskite materials could be better utilized. Secondly, the interpenetration of perovskite and spiro-MeOTAD provided richer interfaces for excitons to separate. These conclusions are in correspondence with the results of incident photon to current conversion efficiency (IPCE), which not only increased in 490–800 nm, but also in the area of <490 nm without enhancement of light absorption.

In order to compare the device performances more objectively, at least 20 individual devices both with and without the rough interface were fabricated and measured under AM 1.5G sun illumination (100 mW cm^{-2}). Fig. 3e shows the average device performance and the error bars based on the structure: FTO/compact TiO_2/mesoporous TiO_2/$CH_3NH_3PbI_3$/spiro-MeOTAD/Ag. Benefiting from the rougher interface of perovskite/HTM, the average J_{sc} increased from 15.3 mA cm^{-2} (Device A) to 16.5 mA cm^{-2} (Device B), with almost unchanged V_{oc} and FF. The average PCE increased from 7.6% to 8.4% as well (Table 1).

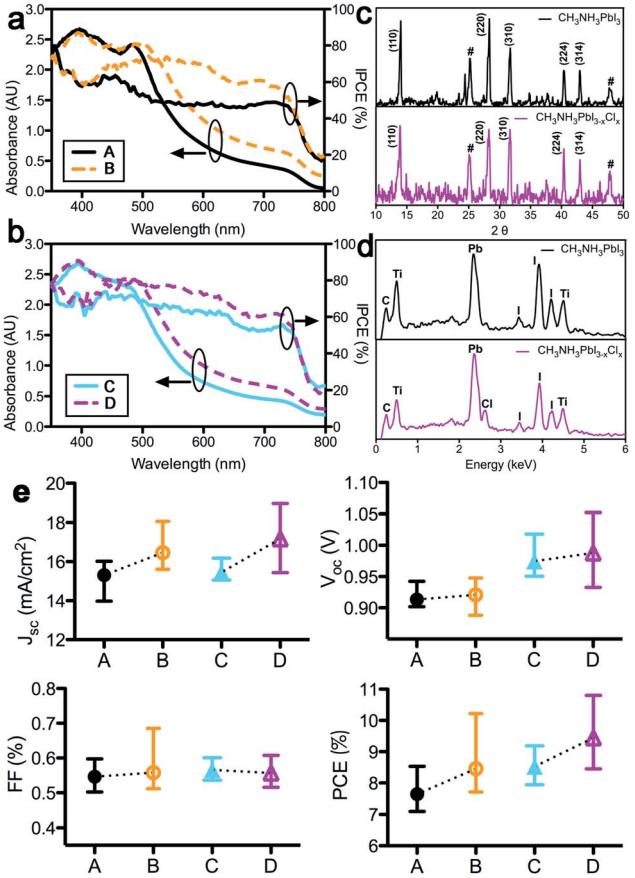

Fig. 3 (a) The absorption spectra and IPCE of (a) $CH_3NH_3PbI_3$ and (b) $CH_3NH_3PbI_{3-x}Cl_x$ device. (c) XRD spectra and (d) EDS spectra of the perovskite films on top of the mesoporous TiO_2, hashes indicate the peaks ascribed to TiO_2. (e) The photovoltaic performances of Devices A–D. Each data point represents the average of a set of at least 20 individual devices.

To exclude the effect brought by different crystal types of perovskite, XRD data were measured to prove the perovskite in the same tetragonal (*I*4/*mcm*) symmetry at both 25 °C and 50 °C (Fig. 3c).[30–32] According to T. Baikie's research, the tetragonal perovskite becomes cubic at the temperatures of 54–57 °C. That is why no temperature higher than 50 °C has been considered as the high reaction temperature.[30]

The conditions to form the rougher interface are also suitable for the Cl-doped hybrid perovskite of $CH_3NH_3PbI_{3-x}Cl_x$ ($x \approx 0.5$, approximately deduced from the energy dispersive spectra (EDS) as shown in Fig. 3d) by sequential deposition. By reacting films of PbI_2–$PbCl_2$ mixtures with CH_3NH_3I at 25 °C (Film C) and 50 °C (Film D), rougher surfaces of the perovskite layers have been obtained in Film D, with the similar SEM image to Film B (Fig. S1†). Obvious higher absorption spectra and IPCE are observed for Device D (from Film D) than Device C (from Film C) over the range of 470–750 nm (Fig. 3b). The maximum IPCE of Device D at 500 nm is over 80%. The average J_{sc} of Device D reached 17.2 mA cm^{-2}, 1.7 mA cm^{-2} higher than that of Device C, with the average PCE increasing from 8.5% to 9.5%. XRD data confirmed no change on crystal type if perovskite crystallites were forming at 50 °C. Compared to $CH_3NH_3PbI_3$ devices, the average J_{sc} of $CH_3NH_3PbI_{3-x}Cl_x$ devices are unanimously larger (Fig. 3e), probably due to the longer charge diffusion length and improved charge transport properties of $CH_3NH_3PbI_{3-x}Cl_x$.[9,32]

Since the control condition to make the rough surface is only about the process of crystal formation, it is also applicable to devices without the mesoporous structure. The devices based on the structure: FTO/compact TiO_2/$CH_3NH_3PbI_3$/spiro-MeO-TAD/Ag were also fabricated by forming $CH_3NH_3PbI_3$ at 25 °C and 50 °C. The rough interface and enhancement of J_{sc} and PCE can be obviously observed for devices under the reaction at 50 °C (Fig. S2†). These results indicate that to introduce a rough interface of perovskite/HTM is a universal way to increase the short-circuit current and PCE of perovskite solar cells without the necessity of mesostructure.

Table 1 The photovoltaic performances[a] of Devices A–G

Device	V_{oc} (V)	J_{sc} (mA cm^{-2})	FF	PCE (%)
A	0.91	15.3	0.55	7.6
B	0.92	16.5	0.56	8.4
C	0.97	15.5	0.57	8.5
D	0.99	17.2	0.56	9.5
E	0.93	14.8	0.45	6.2
F	0.88	17.5	0.48	7.4
G	0.74	15.8	0.49	5.7

[a] The average of a set of at least 20 individual devices. The performances of each device are listed in Table S1.

2. Pre-wetting time control

From the previous conclusions, the rough interfaces of perovskite/HTM are advantageous to the J_{sc}. Meanwhile, controlling the pre-wetting time can also be used to adjust the roughness of surface.[29] By changing the pre-wetting time from 0 s (Film E), 2 s (Film A) to 5 s (Film F) and 10 s (Film G), the perovskite crystallites grew from 100 nm of in-plane grain size for Film E to about 200 nm for Film A, 350 nm for Film F and 1 μm for Film G (Fig. 4), and turned into rough surfaces in Films F and G. Accordingly, the 3D topographic images (Fig. S3b†) displayed gradual increases of roughness with prolonging the pre-wetting time. The calculated rms roughnesses for Films E, A, F, and G, were 44.1 nm, 44.5 nm, 87.8 nm, and 118 nm, respectively

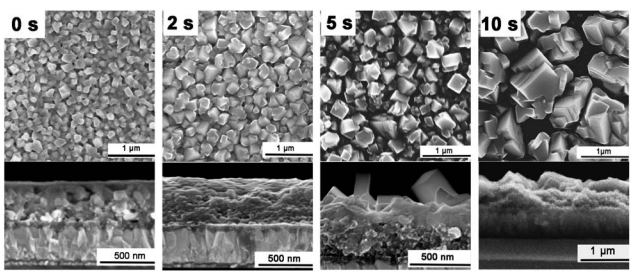

Fig. 4 Top-view and cross-sectional SEM images of the perovskite layer on top of the mesoporous TiO_2 at different pre-wetting times of 0 s, 2 s, 5 s, and 10 s corresponding to Films E, A, F, and G.

(Fig. S3c†). However, the enlargement of perovskite crystallites was accompanied with loose arrangement of the crystallites and the bareness of the mesoporous TiO_2, which was different from the changes taken by temperature.

According to the absorption spectra, Films F and G showed additional absorption than Films A and E, especially Film G, with strong light scattering from 500 nm to 800 nm (Fig. 5a). As a consequence, Device F (from Film F) and Device G (from Film G) displayed distinctly higher J_{sc} than Device A (from Film A), and Device E (from Film E) without pre-wetting showed the poorest J_{sc}. Device F gave the highest average J_{sc} of 17.5 mA cm^{-2}, even 1.7 mA cm^{-2} higher than Device G, although its absorbance was weaker than that of Film G (Fig. 5b). This can be explained by the SEM image of Film G. As the isolated crystallites are with the size of 1 μm, far more than 100 nm of the charge diffusion length of $CH_3NH_3PbI_3$,[9,10] the electron and hole recombination becomes more serious. Crystallites in Devices B and F had the same size of 350 nm, and achieved the highest in each group, indicating that ~350 nm maybe a suitable size of perovskite crystallites for solar cells.[19]

However, Device A showed the highest average PCE of 7.6% with the lowest average J_{sc} of 15.3 mA cm^{-2}. This mismatch derived from the V_{oc} loss caused by the partially direct contacting between the HTM and the bare mesoporous TiO_2 in Devices F and G.[11,33] Hence, high coverage of TiO_2 is crucial and essential to achieve high PCEs, and short pre-wetting time can make sure full coverage of the TiO_2.

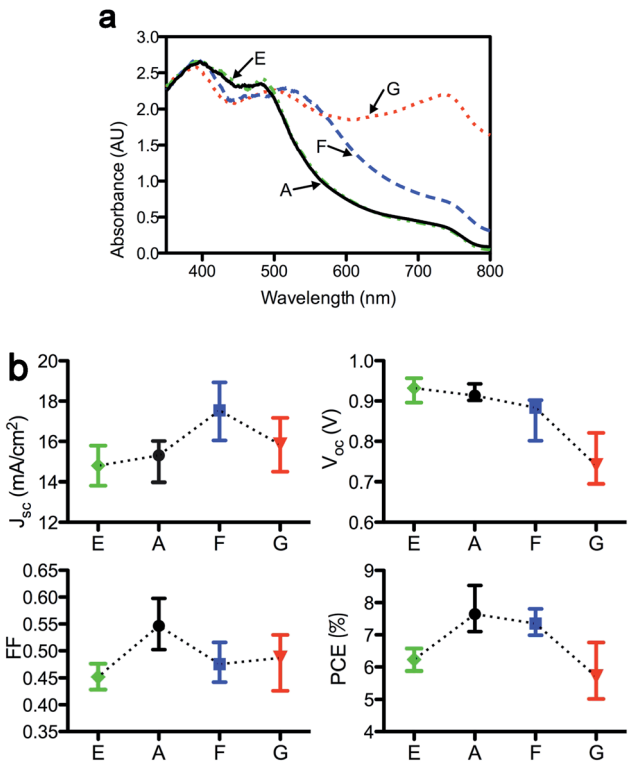

Fig. 5 (a) The absorption spectra of Films E, A, F, and G. (b) The photovoltaic performances of Devices E, A, F, and G. Each data point represents the average of a set of 20 individual devices.

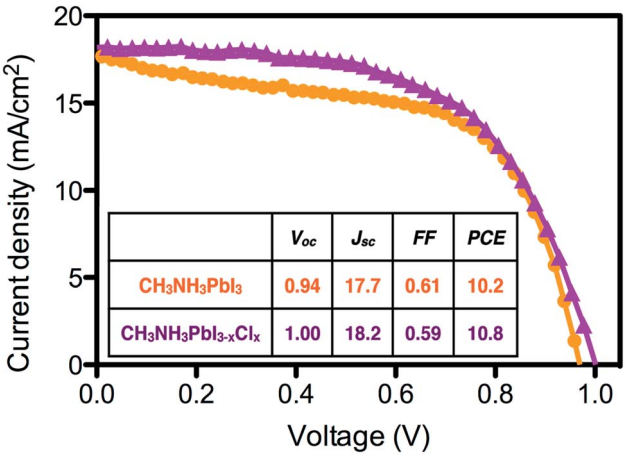

Fig. 6 The best photovoltaic performances of the devices with a rough interface of perovskite/HTM.

Through the control of the pre-wetting time, we also realized the rough interface of perovskite/HTM and the enhancement of J_{sc} by the light scattering. But the continuity of the perovskite film has been destroyed and the TiO_2 was bared, which led to a seriously unfavorable impact on the V_{oc} and PCE. The research of the pre-wetting step reminds us of an important factor which cannot be ignored in fabricating the device with a rough interface.

As the discussion above, the reaction temperature mainly affects the size of perovskite crystallites, while the pre-wetting time affects both the size and compact degree of crystallites. A rough but also continuous interface of perovskite/HTM can be fabricated by the increased reaction temperature and shortened pre-wetting time. Benefiting from improved light absorption and charge transport, the best performances of optimized devices containing a rough interface reached PCEs of 10.2% and 10.8% for $CH_3NH_3PbI_3$ and $CH_3NH_3PbI_{3-x}Cl_x$, respectively (Fig. 6).

Conclusions

In summary, we successfully fabricated the perovskite solar cell containing a rough interface of perovskite/HTM. The pre-wetting time and reaction temperature were systematically investigated to control the morphology of the perovskite film on TiO_2. The expected solar cells with a rough as well as continuous interface of perovskite/HTM were obtained at the higher reaction temperature of 50 °C, with the pre-wetting time of 2 s. Due to the improved light harvesting and charge transporting properties, the J_{sc} and PCE increased simultaneously without changing the thickness and the complexity of the device. Accordingly, the best performing devices have been achieved with PCEs of 10.2% and 10.8% for $CH_3NH_3PbI_3$ and $CH_3NH_3PbI_{3-x}Cl_x$, respectively. This work suggests an effective way for perovskite solar cells to make full use of incident light and improve the charge transporting property. The results have been proved to be consistent for both $CH_3NH_3PbI_3$ and $CH_3NH_3PbI_{3-x}Cl_x$ based solar cells, and it is also appropriate for perovskite solar cells by sequential deposition with various structures.

Experimental details

CH_3NH_3I preparation

Based on the literature,[18] hydroiodic acid (114 mmol, 15 mL, 57 wt%) and methylamine (140 mmol, 70 mL, 2 M in methanol) were reacted at 0 °C with stirring under N_2 for 120 min. The resultant solution was evaporated to give a white precipitate, then washed with diethyl ether and dried under vacuum and used for the following step without further purification.

Device fabrication

Fluorine doped tin oxide (FTO) glass was cleaned sequentially as previously reported[34] *via* detergent, water, acetone, and ethanol under ultrasonication for 15 min, and then treated with O_2 plasma for 15 min. The following procedure was modified based on the literature.[4] A compact TiO_2 layer on the FTO glass was prepared by spin-coating of titanium diisopropoxide bis(acetylacetonate) solution (0.15 M, in 1-butanol) at 4000 r.p.m. for 30 s, dried at 125 °C for 5 min, then repeated twice with 0.3 M of titanium diisopropoxide bis(acetylacetonate) solution, finally baked at 500 °C for 15 min. Then, the resultant TiO_2 film was immersed into a 40 mM $TiCl_4$ aqueous solution at 70 °C for 30 min, washed with deionized water and ethanol, then baked at 500 °C for 15 min. The mesoporous TiO_2 film was prepared by spin-coating a 20 nm-sized TiO_2 paste (diluted in ethanol with a ratio of 2 : 7 by weight, Heptachroma, DHS-TPP3) at 4000 r.p.m. for 30 s, dried at 125 °C for 5 min, then heated at 500 °C for 15 min. The mesoporous TiO_2 films were filled by spin-coating of 1 M PbI_2 solution (Films A, B, E, F, and G) in DMF at 3000 r.p.m. or 1 M PbI_2–$PbCl_2$ (1 : 1) mixed solution (Films C and D) in DMF at 2500 r.p.m. that was kept at 70 °C. After drying at 70 °C, the films were pre-wetted by 2-propanol for 0 s (Film E), 2 s (Films A, B, C, and D), or 5 s (Film F), or 10 s (Film G), before dipping into 10 mg mL^{-1} CH_3NH_3I solution kept at R.T. (Films A, C, E, F, and G) or 50 °C (Films B and D) for tens of seconds. A solution of 2,2′,7,7′-tetrakis(*N*,*N*-di-*p*-methoxyphenylamine)-9,9′-spirobifluorene (spiro-MeOTAD), 4-*tert*-butylpyridine (96%, Aldrich), and lithium bis(trifluoromethylsulphonyl)imide (98%, Alfa Aesar) in chlorobenzene (99.9%, Alfa Aesar) was spin-coated at 2000 r.p.m. for 60 s as the HTM. Finally, 80 nm Ag was thermally evaporated under vacuum to act as the cathode.

Measurements

The absorption spectrum was recorded with a UV-visible spectrophotometer (Agilent 8453). The morphology was measured using a scanning electron microscope (SEM) (FEI Nova_NanoSEM430 and HITACHI 4300) and an atomic force microscope (AFM) (Agilent Series 5500). The EDS spectra were recorded on Nova_NanoSEM430. The XRD spectra were obtained from a Philips X'PERT-MRD X-ray diffractometer. Photovoltaic performances were measured by using a Keithley 2611 source meter under simulated sunlight from an Oriel 300 solar simulator. IPCE was measured by using a lock-in amplifier coupled with a monochromator and a 500 W xenon lamp (Crowntech, Qtest Station 2000). Both the systems were calibrated against a certified reference solar cell. All the measurements of the solar cells were performed under ambient atmosphere at room temperature without encapsulation.

Acknowledgements

This study was partly financially supported by the National Natural Science Foundation of China (10934001, 61177020, 11074016, 11121091, 61275034 and 61106123) and the National Basic Research Program of China (2013CB328700). The authors are thankful to Mr Xiao Yu and Prof. Dechun Zou in the College of Chemistry and Molecular Engineering of Peking University for their kind help in the assistance in the measurements of SEM images.

Notes and references

1 A. Kojima, K. Teshima, Y. Shirai and T. Miyasaka, *J. Am. Chem. Soc.*, 2009, **131**, 6050–6051.
2 M. M. Lee, J. Teuscher, T. Miyasaka, T. N. Murakami and H. J. Snaith, *Science*, 2012, **338**, 643–647.
3 H. S. Kim, C. R. Lee, J. H. Im, K. B. Lee, T. Moehl, A. Marchioro, S. J. Moon, R. Humphry-Baker, J. H. Yum, J. E. Moser, M. Gräztel and N. G. Park, *Sci. Rep.*, 2012, **2**, 591.
4 J. Burschka, N. Pellet, S.-J. Moon, R. Humphry-Baker, P. Gao, M. K. Nazeeruddin and M. Gräztel, *Nature*, 2013, **499**, 316–319.
5 D. Liu and T. L. Kelly, *Nat. Photonics*, 2014, **8**, 133–138.
6 H. J. Snaith, *J. Phys. Chem. Lett.*, 2013, **4**, 3623–3630.
7 W. Zhang, M. Saliba, S. D. Stranks, Y. Sun, X. Shi, U. Wiesner and H. J. Snaith, *Nano Lett.*, 2013, **13**, 4505–4510.
8 P. Qin, A. L. Domanski, A. K. Chandiran, R. Berger, H.-J. Butt, M. l. Dar, T. Moehl, N. Tetreault, P. Gao, S. Ahmad, M. K. Nazeeruddin and M. Gräztel, *Nanoscale*, 2014, **6**, 1508.
9 S. D. Stranks, G. E. Eperon, G. Grancini, C. Menelaou, M. J. P. Alcocer, T. Leijtens, L. M. Herz, A. Petrozza and H. J. Snaith, *Science*, 2013, **342**, 341–344.
10 G. Xing, N. Mathews, S. Sun, S. S. Lim, Y. M. Lam, M. Gräztel, S. Mhaisalkar and T. C. Sum, *Science*, 2013, **342**, 344–347.
11 G. E. Eperon, V. M. Burlakov, P. Docampo, A. Goriely and H. J. Snaith, *Adv. Funct. Mater.*, 2014, **24**, 151–157.
12 T. Leijtens, G. E. Eperon, S. Pathak, A. Abate, M. M. Lee and H. J. Snaith, *Nat. Commun.*, 2013, **4**, 2885.
13 K. Wojciechowski, M. Saliba, T. Leijtens, A. Abate and H. J. Snaith, *Energy Environ. Sci.*, 2014, **7**, 1142.
14 J. H. Noh, S. H. Im, J. H. Heo, T. N. Mandal and S. I. Seok, *Nano Lett.*, 2013, **13**, 1764–1769.
15 H.-S. Kim, J.-W. Lee, N. Yantara, P. P. Boix, S. A. Kulkarni, S. Mhaisalkar, M. Gräztel and N.-G. Park, *Nano Lett.*, 2013, **13**, 2412–2417.
16 M. Liu, M. B. Johnston and H. J. Snaith, *Nature*, 2013, **501**, 395–398.
17 A. Abrusci, S. D. Stranks, P. Docampo, H.-L. Yip, A. K. Y. Jen and H. J. Snaith, *Nano Lett.*, 2013, **13**, 3124–3128.
18 J. H. Heo, S. H. Im, J. H. Noh, T. N. Mandal, C.-S. Lim, J. A. Chang, Y. H. Lee, H.-j. Kim, A. Sarkar,

M. K. Nazeeruddin, M. Gräztel and S. I. Seok, *Nat. Photonics*, 2013, **7**, 486–491.
19 Q. Chen, H. Zhou, Z. Hong, S. Luo, H.-S. Duan, H.-H. Wang, Y. Liu, G. Li and Y. Yang, *J. Am. Chem. Soc.*, 2013, **136**, 622–625.
20 O. Malinkiewicz, A. Yella, Y. H. Lee, G. M. Espallargas, M. Gräztel, M. K. Nazeeruddin and H. J. Bolink, *Nat. Photonics*, 2013, **8**, 128–132.
21 C. Wehrenfennig, G. E. Eperon, M. B. Johnston, H. J. Snaith and L. M. Herz, *Adv. Mater.*, 2014, **26**, 1584–1589.
22 P. Docampo, J. M. Ball, M. Darwich, G. E. Eperon and H. J. Snaith, *Nat. Commun.*, 2013, **4**, 2761.
23 B. Conings, L. Baeten, C. D. Dobbelaere, J. D'Haen, J. Manca and H.-G. Boyen, *Adv. Mater.*, 2014, **26**, 2041–2046.
24 G. Li, V. Shrotriya, J. Huang, Y. Yao, T. Moriarty, K. Emery and Y. Yang, *Nat. Mater.*, 2005, **4**, 864–868.
25 M. Graetzel, R. A. J. Janssen, D. B. Mitzi and E. H. Sargent, *Nature*, 2012, **488**, 304–312.
26 J. Müller, B. Rech, J. Springer and M. Vanecek, *Sol. Energy*, 2004, **77**, 917–930.
27 K. Zhu, N. R. Neale, A. Miedaner and A. J. Frank, *Nano Lett.*, 2007, **7**, 70–74.
28 P. Qiang, P. Yang, Z. Liang, Y. Luo, J. Yu, Y. Lan, X. Cai, S. Tan, P. Liu and W. Mai, *J. Alloys Compd.*, 2014, **583**, 300–304.
29 G. Dhanaraj, K. Byrappa, V. Prasad and M. Dudley, in *Springer Handbook of Crystal Growth*, ed. F. Abbona and D. Aquilano, Springer, Berlin Heidelberg, 2010, pp. 53–87.
30 T. Baikie, Y. Fang, J. M. Kadro, M. Schreyer, F. Wei, S. G. Mhaisalkar, M. Gräztel and T. J. White, *J. Mater. Chem. A*, 2013, **1**, 5628–5641.
31 C. C. Stoumpos, C. D. Malliakas and M. G. Kanatzidis, *Inorg. Chem.*, 2013, **52**, 9019–9038.
32 S. Colella, E. Mosconi, P. Fedeli, A. Listorti, F. Gazza, F. Orlandi, P. Ferro, T. Besagni, A. Rizzo, G. Calestani, G. Gigli, F. D. Angelis and R. Mosca, *Chem. Mater.*, 2013, **25**, 4613–4618.
33 H. J. Snaith, N. C. Greenham and R. H. Friend, *Adv. Mater.*, 2004, **16**, 1641–1645.
34 L. Zhang, X. Xing, Z. Chen, L. Xiao, B. Qu and Q. Gong, *Energy Technol.*, 2013, **1**, 613–616.